NANO · MICRO small
www.small-journal.com

Creation of Nonspherical Microparticles through Osmosis-Driven Arrested Coalescence of Microfluidic Emulsions

*Kai Feng, Ning Gao, Wanlin Zhang, Kang Zhou, Hao Dong, Peng Wang, Li Tian, Guokang He, and Guangtao Li**

Droplet-based microfluidics enable the production of emulsions and microparticles with spherical shapes, but the high-throughput fabrication of nonspherical emulsions and microparticles still remains challenging because interfacial tension plays a dominant role during preparation. Herein, ionic liquids (ILs) containing salts, which possess sufficient osmotic pressure to realize water transport and phase separation, are introduced as inner cores of oil-in-oil-in-water double emulsions and it is shown that nonspherical emulsions can be constructed by osmosis-driven arrested coalescence of inner cores. Subsequently, ultraviolet polymerization of the nonspherical emulsions leads to nonspherical microparticles. By tailoring the number, composition, and size of inner cores as well as coalescence time, a variety of nonspherical shapes such as dumbbell, rod, spindle, snowman, tumbler, three-pointed star, triangle, and scalene triangle are created. Importantly, benefitting from excellent solvency of ILs, this system can serve as a general platform to produce nonspherical microparticles made from different materials. Moreover, by controlling the osmotic pressure, programmed coalescence of inner cores in double emulsions is realizable, which indicates the potential to build microreactors. Thus, a simple and high-throughput strategy to create nonspherical microparticles with arrested coalescence shapes is developed for the first time and can be further used to construct novel materials and microreactors.

1. Introduction

Microparticles find widespread applications in various fields such as delivery carriers for drugs,[1] building blocks in tissue engineering, and research object of self-assembly.[2,3] The properties and functions of microparticles are decided by many parameters in which shape is supposed to be a critical one.[4–6] Among methods of preparing microparticles, droplet microfluidics is regarded as an efficient strategy for large-scale fabrication of a variety of emulsions and materials on the micrometer scale.[7–9] This technology enables the production of various emulsions and microparticles with spherical shapes,[10] but the high-throughput fabrication of nonspherical emulsions and microparticles still remains challenging because interfacial tension plays a dominant role on the micrometer scale. Compared with spherical microparticles, anisotropic nonspherical microparticles offer unique properties and functions and are of wide applications in cosmetics,[11] biotechnology,[12] structural materials,[13] and pharmaceuticals.[14] Several strategies to fabricate nonspherical microparticles have been developed in microfluidic systems. One of these methods is based on the deformation of spherical emulsions through external forces and nonspherical shapes are captured by polymerization.[6,15,16] Various nonspherical structured liquids are also fabricated and maintained by nanoparticle–polymer surfactants or interfacial jamming of nanoparticles.[17–19] Anisotropic bijel (bicontinuous interfacially jammed emulsion gels) microparticles are formed by jammed colloidal particles at the interface.[20] But these means generate limited nonspherical shapes and cannot meet the demand for creating microparticles with complex nonspherical shapes. Advances in flow lithography technology enable the production of microparticles with various well-controlled shapes, but the morphology is strictly dependent on the instrument and mold geometry.[21–23] Assembly strategy from building blocks is also developed to construct microparticles with nonspherical shapes.[24–27] Besides, liquid bridge method and capillary origami method are exploited to fabricate complex 3D shapes.[28,29] Using liquid crystalline elastomers, highly shape-anisotropic particles in response to a certain external stimulus are synthesized by microfluidics.[30] However, these assembly and fabrication methods are often time-consuming and the productivity and shape complexity still need to be improved. Arrested coalescence of Pickering emulsions and viscoelastic droplets is also studied to construct nonspherical structures, but the arrested coalescence is not a spontaneous process and depends strictly on manual operation, which cannot be realized on a large scale by far, limiting its application in large-scale production.[31–33] Despite significant advances in this field with regard to preparing nonspherical microparticles,[34] a

K. Feng, Dr. N. Gao, W. Zhang, K. Zhou, H. Dong, P. Wang, L. Tian, G. He, Prof. G. Li
Department of Chemistry
Key Lab of Organic Optoelectronics & Molecular Engineering
Tsinghua University
Beijing 100084, China
E-mail: lgt@mail.tsinghua.edu.cn

The ORCID identification number(s) for the author(s) of this article can be found under https://doi.org/10.1002/smll.201903884.

DOI: 10.1002/smll.201903884

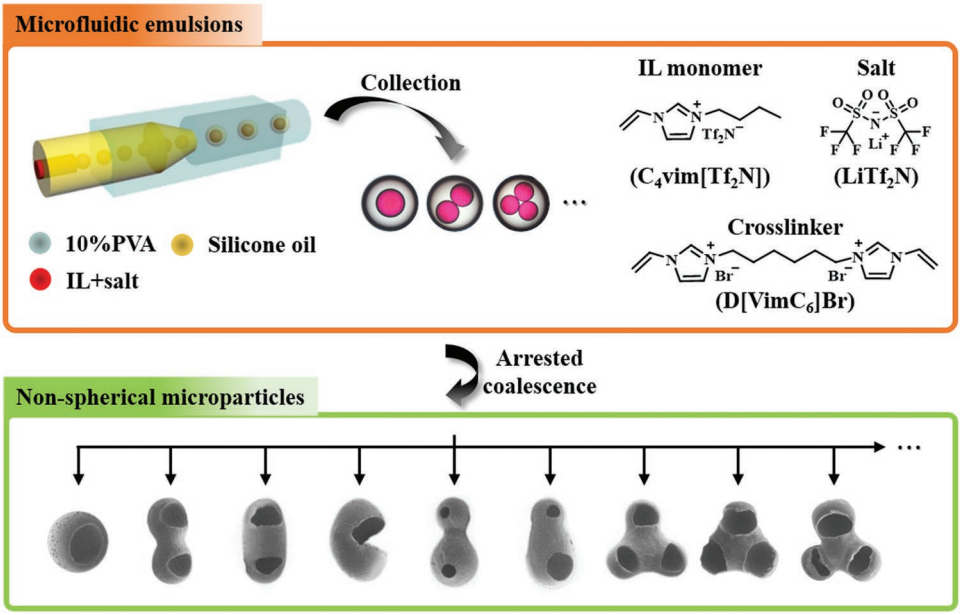

Figure 1. Schematic illustration of the generation of O/O/W double emulsions by microfluidics and creation of diverse nonspherical microparticles through osmosis-driven arrested coalescence.

simple and high-throughput method to fabricate multiple nonspherical microparticles is still needed.

Osmotic pressure is a thermodynamic driving force that controls the transit of solvent molecules across a semipermeable membrane.[35] In creatures, osmotic pressure plays important roles in cell morphology, water transport, and signal transmission.[36,37] It is also widely applied in industry field, such as power production and water purification.[38,39] Moreover, as an important driving force, osmotic pressure has been exploited to drive fluid exchange and fabricate various materials. For example, solid and flexible photonic capsules for various photonic applications are prepared by osmolarity-controlled annealing method.[40,41] High-order all-aqueous emulsion drops can be generated taking advantage of osmosis-driven phase separation.[42] Using osmotic pressure, swelling behaviors of water-in-oil-in-water (W/O/W) double emulsions are studied.[43,44] In addition, osmotic pressure is exploited to control drug release by swelling-breakdown phenomenon.[45,46] Up to now, however, osmosis is restricted to control water transport between two aqueous phases. The osmotically driven water transport in oil phases for construction of novel materials has seldom been reported owing to poor solubility of osmolyte in conventional organic oils. Recently, our group develops an oil system composed of ionic liquids (ILs) containing salts (ILs/salts) which are of enough osmotic pressure to drive water transport from the aqueous phase to the oil phase, greatly broadening the application of osmotic pressure for creating new materials.[47]

In this paper, based on unique properties of the developed ILs/salts system, we report the creation of nonspherical emulsions by osmosis-driven arrested coalescence of inner cores in oil-in-oil-in-water (O/O/W) double emulsions and prepare nonspherical microparticles using these emulsions as templates. The microfluidic technology allows for facilely generating monodisperse and well-defined O/O/W double emulsions, as shown in **Figure 1**. In the O/O/W double emulsions, an IL (1-butyl-3-vinylimidazolium bis(trifluoromethanesulfonyl) imide, C_4vim[Tf_2N]) containing salt (bis(trifluoromethane)sulfonimide lithium, LiTf_2N) oil solution (C_4vim[Tf_2N]-LiTf_2N) developed by our group is used as the inner oil phase, which possesses sufficient osmotic pressure to realize the water transport from the outer aqueous phase to the inner oil phase, triggering spontaneous phase separation in the inner oil phase.[47] During the water transport and phase separation process, the volume of the inner oil phase gradually increases due to the water absorption. Moreover, the inner/middle oil phase interface becomes instable because of continuous water transport and phase separation through the phase interface. When multi-core O/O/W double emulsions are created, the continuous increase of inner core volume and interfacial instability lead to arrested coalescence of inner cores and nonspherical emulsions are fabricated. Subsequently, ultraviolet (UV) polymerization arrests the emulsions to nonspherical microparticles. By tailoring the number, composition, and size of inner cores in the O/O/W double emulsions as well as coalescence time, a variety of nonspherical microparticles are created (Figure 1). More importantly, we find that the ILs/salts system exhibits remarkable extendibility which can be used as a general platform to prepare nonspherical microparticles of different functions and different materials. In addition, by modulating the osmotic pressure of different cores, programmed sequential coalescence of cores is realizable, showing the potential of these double emulsions as microreactors. To the best of our knowledge, the high-throughput creation of various nonspherical microparticles with arrested coalescence shapes has never been reported before. Unlike all the above reported strategies, in our case, nonspherical emulsions and corresponding microparticles are created by spontaneous arrested coalescence of droplets, which avoids complicated fabrication process. Meanwhile, benefitting

from the microfluidic strategy, a great amount of monodisperse nonspherical microparticles can be prepared in a short time. Notably, through the ILs/salts system and facile adjustment of the preparation conditions, abundant metastable states of emulsions are captured, generating tremendous unexplored structures, which are difficult to accomplish by other means.

2. Results and Discussion

2.1. Formation of O/O/W Double Emulsions and Process of Osmosis-Driven Water Transport and Phase Separation

In order to study the osmosis-driven water transport and phase separation of the ILs/salts system, monodisperse O/O/W double emulsions were produced by glass capillary microfluidic devices. The outer phase was an aqueous solution of 10 wt% poly(vinyl alcohol) (PVA, low M_w). The inner oil phase was a mixture of C_4vim[Tf_2N] and LiTf_2N (5:1, mol/mol) with 1 wt% 1,6-di(*N*,*N*′-vinylimidazolium) hexane dibromide (D[vimC_6]Br) as crosslinker and 1 wt% 2-hydroxy-2-methylpropiophenone (HMPP) as photoinitiator. Rhodamine B was added into the inner oil phase for better observation. The middle oil phase consisted of silicone oil (100 cSt) and polydimethylsiloxane (PDMS) (7:3, w/w) with 4 wt% Dow Corning 749 as surfactant. The silicone oil phase was used to separate the inner and outer phases and allowed for water transport when emulsions were subjected to an osmotic pressure difference.[48] O/O/W double emulsions were generated and collected in a 10 wt% PVA aqueous solution.

The extraordinary solubility of salt (LiTf_2N) in the IL (C_4vim[Tf_2N]) results from the unique physical chemistry properties and multiple molecular interactions of ILs.[49–52] Different from conventional organic solvents, ILs are a class of molten salts consisting of organic cations and anions, exhibiting dual ionic and organic nature and excellent solvency for a broad range of substances.[53–55] Besides, the coordination of Li^+ by oxygen atoms of Tf_2N^- greatly promotes the dissolution of LiTf_2N in C_4vim[Tf_2N].[49] Thus, the inner oil phase dissolving large amounts of inorganic salts (LiTf_2N) owns high osmotic pressure. Using the isotonic solution method (see the Experimental Section), we determined the osmotic pressure of ILs/salts (IL:salt = 5:1, mol/mol) as 1.4×10^4 kPa. Once these O/O/W double emulsions are exposed to the outer aqueous solution, water transport occurs from the outer aqueous phase to the inner oil phase driven by the osmotic pressure difference. Simultaneously, phase separation takes place because C_4vim[Tf_2N] is insoluble with water. In a typical experiment, initially, a lot of dispersive tiny aqueous droplets were absorbed into the inner oil phase and these tiny aqueous droplets gradually coalesced into a giant aqueous droplet (newly formed aqueous phase), as illustrated in **Figure 2**a–c. It should be mentioned that not all tiny aqueous droplets coalesced into the newly formed aqueous phase. A few tiny aqueous droplets still exited alone which were exhibited as tiny bright white spheres in optical microscope images. As shown in Figure 2b,c, during the water transport and phase separation process the diameter of the inner oil phase increased from 434 μm at the beginning to 507 μm after 12 h (see the detailed process in Figure S1, Supporting Information). The prepared emulsions were polymerized by UV light (365 nm, 200 W) for 30 min, and then washed with deionized water, ethanol, and petroleum ether three times to remove PVA and silicone oil. After drying, poly(ionic liquid) (PIL) microcapsules were acquired, as shown in Figure 2d. It was noticeable that a hole appeared after the IL was polymerized (see Figure 2e). This is because of the mismatch of density between the inner oil phase (namely, the IL phase) and the newly formed aqueous phase, resulting in the decentration of the aqueous droplet in the inner oil droplet. During polymerization, the polymerizable inner oil droplet shrinks and the newly formed aqueous droplet inside is squeezed out, leaving cracked holes on microcapsules.[56] The tiny holes distributing on the outer surface of the PIL microcapsules arise from the tiny aqueous droplets which do not coalesce into the newly formed aqueous phase, as shown in Figure 2e. The polymerization-induced holes endow PIL materials with more shape complexities and extensional space.

To better understand the water transport property between the outer aqueous phase and the inner oil phase, we used different inner oil phases (including different salt concentrations and different core sizes) to carry out the water absorption process, as shown in Figure 2f,g. Specifically, the absorbed water volume of the inner oil phases at different salt concentrations (IL:salt = 5:2, 5:1, 5:0.5, mol/mol) versus time was quantificationally studied. Time-sequence optical microscope images were captured during the water absorption process. The initial diameter of the inner core (D_0) and the diameter of the inner core after water absorption for t minutes (D_t) were determined by analyzing the captured images. The volume of the absorbed water (V) was calculated by the following formula: $V = \frac{\pi}{6}(D_t^3 - D_0^3)$. As shown in Figure 2f, the volume of the newly formed aqueous phase increased quickly at the beginning and gradually reached the maximum value and the speed of water transport, on the contrary, decreased with time. This is because that the osmotic pressure difference between the inner oil phase and the outer aqueous phase is maximal initially and decreases to the equilibrium value with more and more water absorbed into the inner oil phase. In addition, emulsions with bigger cores absorbed water more quickly because of higher driving force, as illustrated in Figure 2g. The results indicate that the osmosis-driven water transport and phase separation behaviors could be easily tuned by adjusting the preparation conditions. More importantly, the water transport and phase separation of O/O/W double emulsions make contribution to volume increase of inner cores and instability of inner/middle oil phase interfaces which are crucial to realize arrested coalescence to be discussed below.

2.2. Osmosis-Driven Arrested Coalescence of Dual-Core O/O/W Double Emulsions

As aforementioned, single-core O/O/W double emulsions could be supposed to eventually become W/O/O/W triple emulsions due to the newly formed aqueous phase by osmosis-driven water transport and phase separation, and PIL microcapsules with holes were prepared. Interestingly, when dual-core O/O/W double emulsions were created, arrested coalescence was found

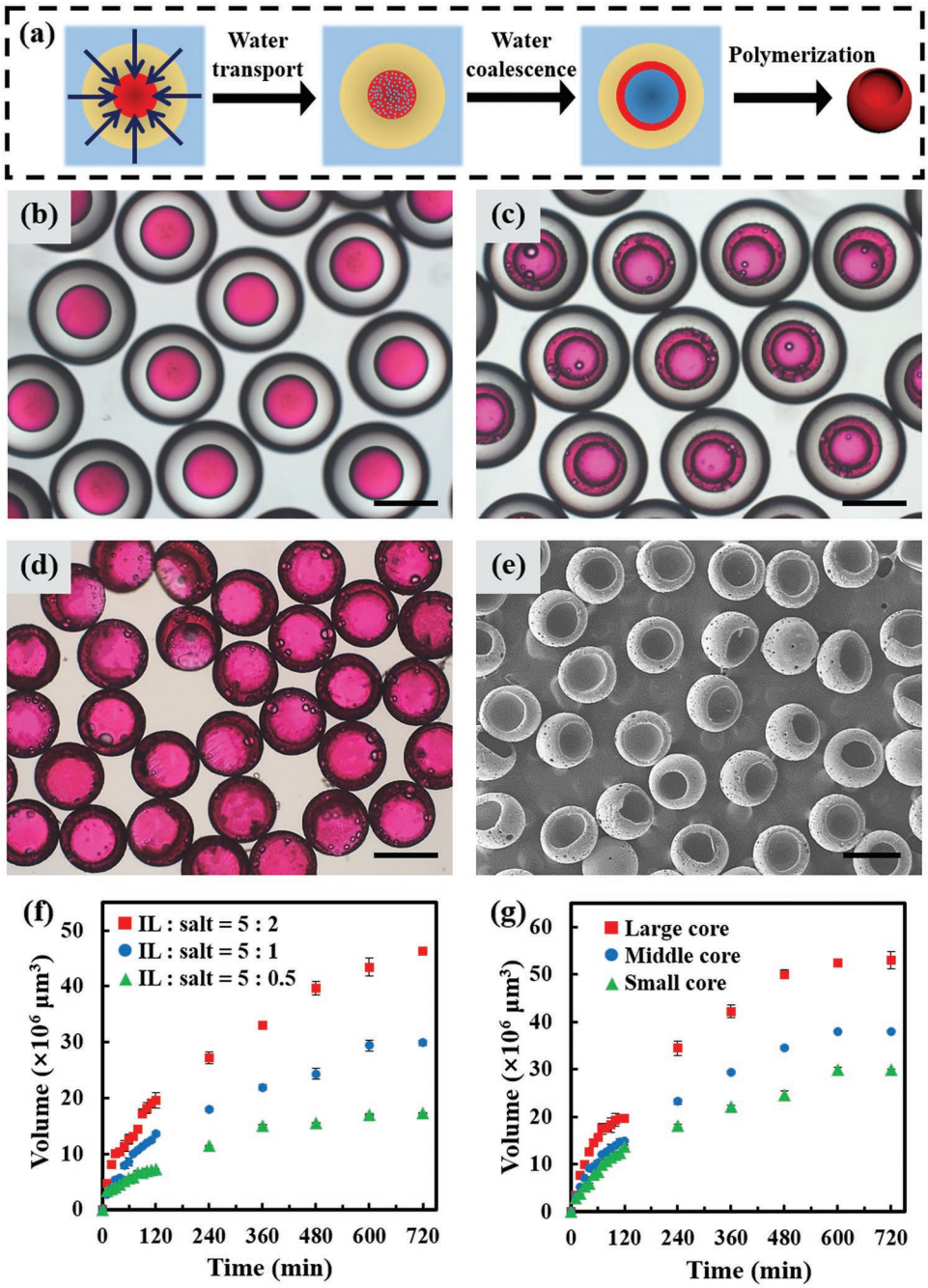

Figure 2. a) Schematic diagrams of the water transport and phase separation process of single-core O/O/W double emulsions. b–e) Optical microscope images of single-core O/O/W double emulsions after b) collection, c) 12 h still standing in the outer aqueous phase, d) polymerization, and e) SEM images of resultant microcapsules with holes. f,g) Variation with time of the absorbed water volume at f) different salt concentrations and g) different core sizes. All scale bars are 500 μm.

between two inner cores during the water transport and phase separation process, as schematically illustrated in **Figure 3**a. Similar to the case in single-core O/O/W double emulsions, water transport occurred from the outer aqueous phase to the inner oil phase in the beginning, leading to the formation of new aqueous phase inside inner cores (Figure 3c,d). After that, instead of being stable, the two cores in the double emulsion partly coalesced and formed a nonspherical emulsion. Figure 3e shows optical microscope images of dual-core O/O/W double emulsions after collection for 10 h. More surprisingly, this partial coalescence state could last for several days. Therefore, using photo-polymerization PIL doublets with arrested coalescence shapes were acquired, as shown in Figure 3f–j. For the same reason with PIL microcapsules, polymerization-induced holes were appeared on each side of the PIL doublet, making the doublet looks like a peanut. To our knowledge, this unique

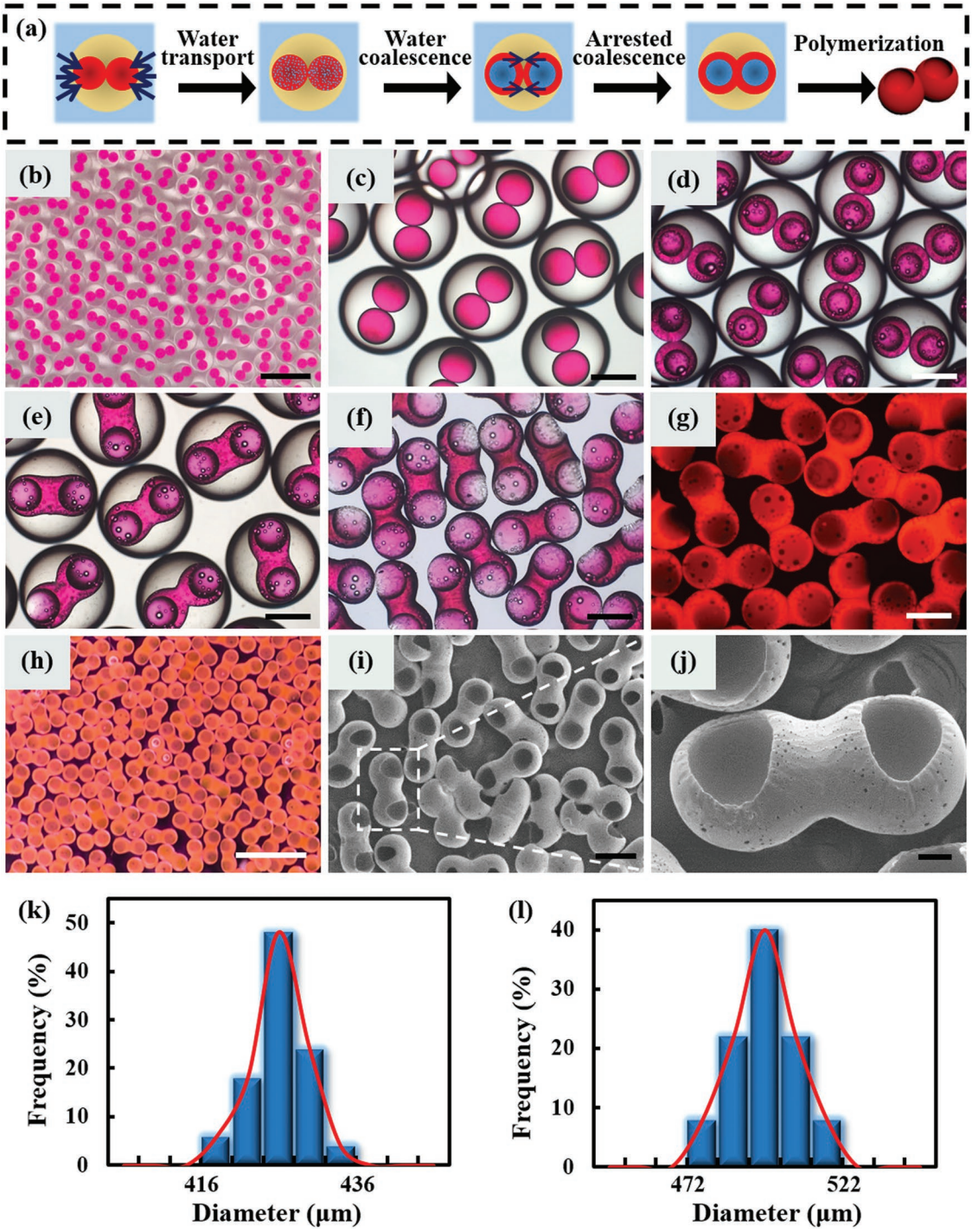

Figure 3. a) Schematic diagrams of arrested coalescence process of dual-core O/O/W double emulsions. b) Optical images of dual-core O/O/W double emulsions after collection, which can be produced on a large scale. c–e) Optical microscope images of dual-core O/O/W double emulsions after collection for c) 0 h, d) 1 h, and e) 10 h. f) Optical microscope images of PIL doublets after polymerization. g) Fluorescence microscope images of PIL doublets. h) Optical images of large amounts of PIL doublets. i,j) SEM images of the fabricated PIL doublets. k,l) Size distribution of inner cores in dual-core O/O/W double emulsions after k) collection and l) polymerization. Scale bars are 2 mm in (b), 500 μm in (c)–(g), 2 mm in (h), 500 μm in (i), and 100 μm in (j).

structure has never been reported before. In addition, all emulsions and microparticles show nice monodispersity benefitting from the microfluidic strategy (Figure 3k,l).

Generally, all emulsion droplets exist individually with each other because of surfactants assisted stabilization, and under shaking, electric stimulus, or other demulsification conditions,

emulsion droplets may coalesce into bigger spherical droplets.[57] Arrested coalescence of emulsions, however, is a thermodynamically metastable state which is difficult to capture. It is realized here using our ILs/salts system in which the coalescence process of inner cores in double emulsions is triggered and arrested, creating nonspherical emulsions and microparticles. This interesting phenomenon can be attributed to the following reasons. First, spatial confinement provides the prerequisite for arrested coalescence. The inner cores are precisely confined in the middle oil phase by the microfluidic emulsification process. During the water transport and phase separation caused by osmotic pressure difference, the diameter of inner cores increases. As a result, the inner cores squeeze against each other due to the confinement of the middle phase, which provides the possibility for arrested coalescence. Second, the triggering of coalescence between adjacent inner cores is supposed to stem from continuous water transport and phase separation through the inner/middle oil phase interface. Unlike traditionally stable double emulsions, O/O/W double emulsions prepared in our work cannot maintain their original morphology because huge difference of osmotic pressure between the inner oil phase and the outer aqueous outer phase drives water transport and phase separation. The process not only leads to the formation of the newly formed aqueous phase inside the inner oil phase, but more significantly, disturbs the inner/middle oil phase interface continuously.[58] As aforementioned, inner cores here are spatially adjacent and therefore coalescence between cores is triggered under interfacial disturbance. Indeed, the arrested coalescence is a more complex process. The complete and comprehensive mechanism is still being studied further and we believe that it must be related to the spatial effect and interfacial instability. To verify the necessity of osmosis in the system, we generated dual-core O/O/W double emulsions in which pure ILs were used as the inner oil phase instead of the IL and salt mixture. In this case, the osmotic pressure difference between the inner oil phase and the outer aqueous phase was negligible. As a result, the osmosis-driven water transport and corresponding phase separation would not take place. After 24 h evolution in the outer aqueous phase, no coalescence was observed (Figure S2, Supporting Information). It should be noted that there was still a little water absorbed into the inner oil phase which resulted from the slight solubility of water in the IL. This control experiment confirms the necessity of osmosis-driven water transport and phase separation for arrested coalescence.

Another key to realize arrested coalescence depends on the capture of coalescence process, otherwise complete coalescence to spherical emulsions will take place at once. In our system, two factors make contribution to arrest the coalescence of inner cores. For one thing, ILs dissolving salts are of high viscosity, which offers the rheological resistance offsetting the interfacial tension. Thus, coalescence process is greatly slowed down and the capture of metastable emulsions becomes possible. To quantify this, we measured the viscosity of ILs/salts (Figure S3, Supporting Information). The viscosity of ILs/salts varied from 229.09 mPa s (IL:salt = 5:2, mol/mol), 123.81 mPa s (IL:salt = 5:1, mol/mol), 100.81 mPa s (IL:salt = 5:0.5, mol/mol) to 65.74 mPa s (pure IL) at 25 °C. The interfacial tension between the inner and middle oil phase was measured as 3.61 mN m^{-1} (Figure S4, Supporting Information). The viscosity of ILs/salts is much higher than traditional solvents (e.g., η_{water} = 0.89 mPa s, $\eta_{toluene}$ = 0.56 mPa s, 25 °C) while the interfacial tension between the inner and middle oil phase is lower than the interfacial tension of conventional oil/water (e.g., $\gamma_{water\text{-}toluene}$ = 35 mN m^{-1}). Interfacial tension is the driving force for the complete coalescence of droplets while viscous force obstructs the coalescence process because of rheological resistance.[59,60] As can be analyzed from the abovementioned results, high viscosity and low interfacial tension slow down the coalescence process and the capture of coalescence process becomes possible. To further study the effect of the viscosity, a less viscous ILs/salts system, consisting of 1-butyl-3-methylimidazolium bis(trifluoromethanesulfonyl)imide (C_4mim[Tf_2N]) and LiTf_2N (5:1, mol/mol), was used to carry out the same experiment. Compared with C_4vim[Tf_2N] in original ILs/salts system, C_4mim[Tf_2N] was less viscous because of the replacement of vinyl by methyl. Both the original ILs/salts system and the less viscous ILs/salts system had the same osmotic pressure, but the latter had lower viscosity. As expected, in the less viscous ILs/salts system it took less time to realize arrested coalescence and shape readjustment (Figure S5, Supporting Information), which indicated that high viscosity obstructed the coalescence process. For another, the newly formed aqueous droplets during water transport and phase separation process contribute to keeping the nonspherical structures of emulsions. Each aqueous droplet forms separately inside its own core during the water transport and phase separation period. Therefore, aqueous droplets locate in their own inner cores after coalescence and act as a skeleton, preventing inner cores from complete coalescence. All in all, due to the spatial adjoining through microfluidic encapsulation, interfacial instability caused by water transport and phase separation, and the balance between interfacial tension and rheological resistance, arrested coalescence is triggered and captured, producing nonspherical emulsions and corresponding microparticles. Different from previously reported methods,[31–33] arrested coalescence by our strategy is an osmosis-driven spontaneous process and can be realized on a large scale by microfluidics.

It should be mentioned that if time is long enough, arrested coalescence would eventually evolve into complete coalescence and nonspherical emulsions become thermodynamically stable spherical emulsions. In our system, when dual-core O/O/W double emulsions were placed in the outer aqueous phase for 3 days, the two newly formed aqueous droplets in the double emulsion merged into one bigger aqueous droplet and two inner oil cores merged into one spherical oil droplet (Figure S6a–d, Supporting Information). It shows that the metastable state of emulsions of the ILs/salts system can last for as long as several days.

Based on the initial results, the O/O/W double emulsions' whole evolution process from individual emulsion droplets to arrested coalescence to eventually complete coalescence lasts for several days. Therefore, by tailoring coalescence time, nonspherical emulsions and microparticles with different degrees of coalescence can be captured. For dual-core O/O/W double emulsions, we captured three different coalescence states at 10, 16, and 24 h after collection. Emulsions captured at 10 h generated dumbbell-like emulsions and microparticles (Figure 3). As

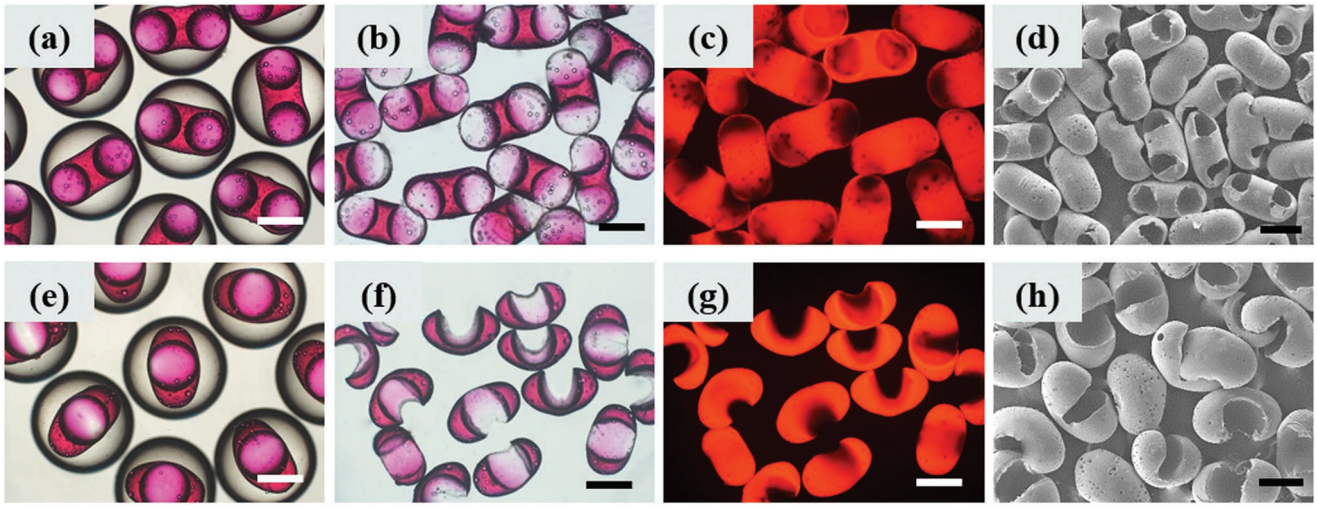

Figure 4. a) Optical microscope images of dual-core O/O/W double emulsions after collection for 16 h. b–d) Optical, fluorescence, and SEM images of PIL doublets of 16 h still standing. e) Optical microscope images of dual-core O/O/W double emulsions after collection for 24 h. f–h) Optical, fluorescence, and SEM images of PIL doublets of 24 h still standing. All scale bars are 500 μm.

time went on, the coalescence area gradually extended. When it came to 16 h, the inner oil phase became rod-like, as shown in **Figure 4**a–d. Next, newly formed aqueous droplets inside the inner oil phase merged together which made the emulsion look like spindle after 24 h evolution in the outer aqueous phase (Figure 4e–h). By UV polymerizing the emulsions at different time, we got PIL doublets with different degrees of coalescence. Benefitting from the long time needed for complete coalescence of inner cores, we theoretically can capture every coalescence state by polymerizing at the exact time, which is hard to realize in other systems.

Taking advantage of the microfluidic strategy, the diameters and composition of the inner cores in O/O/W double emulsions can be flexibly modulated. In this way, we can easily engineer microparticles with designed size and function anisotropy. In the O/O/W double emulsions, sizes of cores can be easily tuned independently by controlling the injection flow rate of each inner oil phase (Figure S7, Supporting Information). By this way, anisotropic snowman-like doublets were created (**Figure 5**a–d). What is more, we could adjust the core sizes as well as coalescence time at the same time. Thus, snowman-like PIL doublets became tumbler-like doublets when the coalescence time was extended from 10 to 18 h, as shown in Figure 5e–h. Additionally, we doped carbon dots inside one inner core of the dual-core O/O/W double emulsion. The resultant emulsions presented half blue fluorescence under UV, which showed the function anisotropy (Figure 5i–m). Nano-sized carbon dots were introduced here because of their fluorescence performance and slow diffusion after arrested coalescence. Although rhodamine B also has good fluorescent performance, it is small molecule and diffuses very quickly in the inner core. If rhodamine B was doped into one of the inner cores, the function anisotropy would not be preserved after the arrested coalescence of the inner core because of the rapid diffusion of the rhodamine B. These structures acquired through facile adjustment of preparation conditions endow materials with more anisotropic characteristics.

2.3. Osmosis-Driven Arrested Coalescence of Triple-Core O/O/W Double Emulsions

Having the results of dual-core O/O/W double emulsions, we extended to triple-core O/O/W double emulsions. The core number of double emulsions could be tuned by simply adjusting flow rates during the microfluidic process. The arrested coalescence of triple-core O/O/W double emulsions was similar to the process in dual-core double emulsions, as shown in **Figure 6**a. Water transport took place from the outer aqueous phase to the three inner cores, leading to the formation of the newly formed aqueous phase in each inner core. Next, arrested coalescence of three cores in each emulsion occurred spontaneously after 10 h evolution in the outer aqueous phase, forming three-pointed star emulsions. By UV polymerization, PIL triplets were prepared each of which contained three holes. Figure 6b–j shows the optical, fluorescence, and scanning electron microscope (SEM) images during the fabrication process. The PIL triplet exhibits well-defined structure which stems from uniform emulsions generated by microfluidics (Figure 6k,l).

Similarly, triple-core O/O/W double emulsions could also generate PIL triplets with different degrees of coalescence through adjusting coalescence time. PIL triplets acquired by polymerizing at 10 h seemed like three-pointed stars (see Figure 6e–j) while looked more like triangles at 22 h (see **Figure 7**a–d). When triple-core O/O/W double emulsions were placed in the outer aqueous phase for 3 days, triple-core O/O/W double emulsions also evolved into spherical W/O/O/W triple emulsions finally (Figure S6e–h, Supporting Information). To fabricate triple-core O/O/W double emulsions with cores of different sizes, three inner phases were injected separately. Thus, scalene triangle microparticles were created, as shown in Figure 7e–h.

Droplet-based microfluidics provides a versatile platform for generating well-defined microemulsions, which are good candidates for us to effectively synthesize a myriad of nonspherical

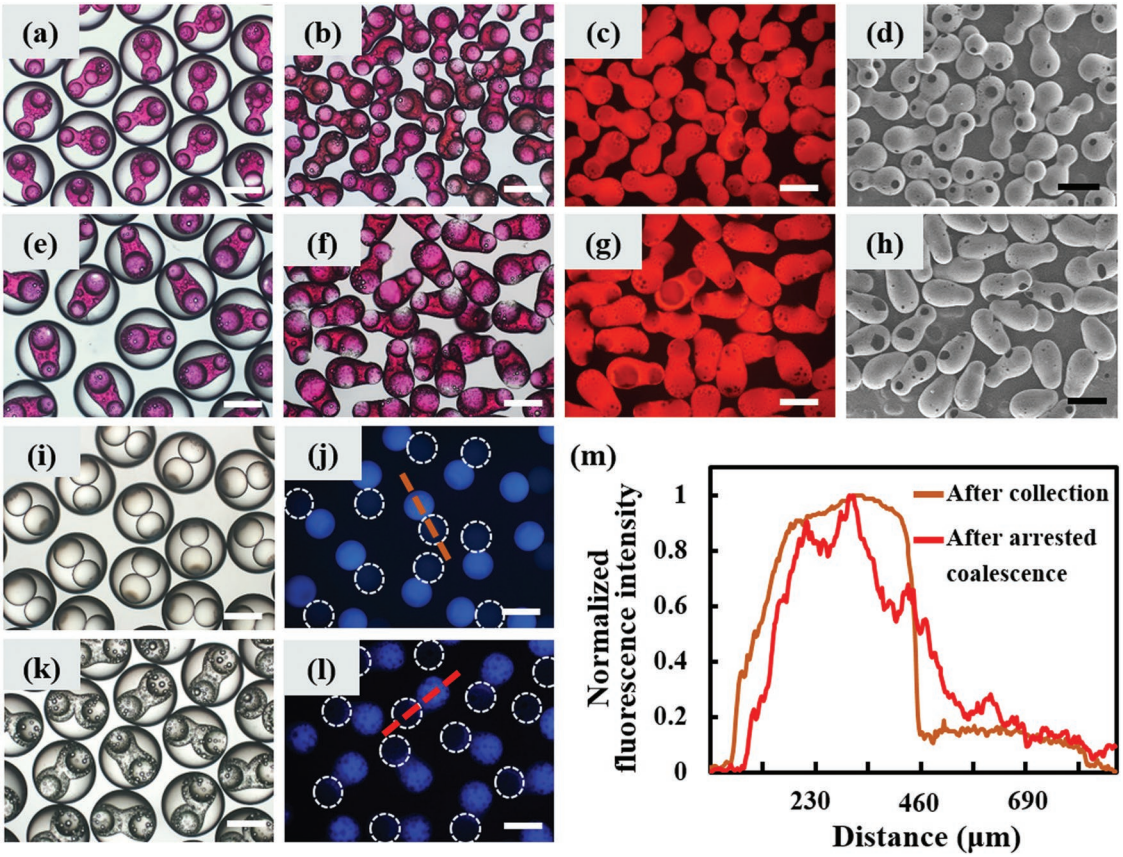

Figure 5. a) Optical microscope images of dual-core O/O/W double emulsions with cores of different sizes after collection for 10 h. b–d) Optical, fluorescence, and SEM images of snowman-like PIL doublets. e) Optical microscope images of dual-core O/O/W double emulsions with cores of different sizes after collection for 18 h. f–h) Optical, fluorescence, and SEM images of tumbler-like PIL doublets. i,j) Optical and fluorescence microscope images of dual-core O/O/W double emulsions after collection in which one core was doped with carbon dots. k,l) Optical and fluorescence microscope images of dual-core O/O/W double emulsions after arrested coalescence in which one core was doped with carbon dots. m) Fluorescent profiles along broken lines in (j) and (l). All scale bars are 500 μm.

microparticles. Although only dual-core and triple-core O/O/W double emulsions are exploited to create various nonspherical microparticles in this work, a variety of more complex double emulsions can be fabricated using microfluidic strategy such as multi-cored microcapsules,[61–63] which means that our strategy is able to be extended for creating more abundant nonspherical microparticles. What is more, Doyle and co-workers developed a flow lithography method for high-throughput microparticle synthesis.[21–23] We trust the combination of lower viscosity IL mixtures with the flow lithography method would be a great advantage to the efficient preparation of various nonspherical microparticles.

2.4. Remarkable Extendibility of the ILs/Salts System

Due to the multiple interactions, ILs exhibit peculiar ability to dissolve a broad range of substances,[53–55] which implicates that the ILs/salts system could serve as a general platform to fabricate various functional nonspherical microparticles. As a proof of our concept, aggregation-induced emission (AIE) molecule (tetraphenylethylene luminogen, **Figure 8**a) was dissolved in C_4vim[Tf_2N]-LiTf_2N. The addition of the AIE molecule did not affect the water transport, phase separation, and arrested coalescence of O/O/W double emulsions. After arrested coalescence, the AIE molecule was co-polymerized with the IL under UV. Thus, AIE-doped PIL doublets and triplets were created and the resultant nonspherical microparticles exhibited blue fluorescence under UV, as described in Figure 8b–e. The result shows that nonspherical microparticles created through our strategy can be functionalized simply by dissolving or dispersing functional species in the IL.

Although a series of nonspherical microparticles is prepared above, they are all PIL materials. Further, we extend our strategy to create nonspherical microparticles made from other materials. In this case, the polymerizable IL (C_4vim[Tf_2N]) was replaced by unpolymerizable C_4mim[Tf_2N], and ethoxylated trimethylolpropane triacrylate (ETPTA, Figure 8f) was used as the monomer and crosslinker. The inner oil phase here was consisted of 67 wt% C_4mim[Tf_2N], 17 wt% ETPTA, and 15 wt% LiTf_2N with 1 wt% HMPP as photoinitiator. The osmosis-driven arrested coalescence of O/O/W double emulsions was not influenced by the dissolution of 17 wt% ETPTA. Therefore, doublets and triplets were created through the same process and the difference was that they were made from polymerized ETPTA (PETPTA) instead of PIL. After polymerization, PETPTA doublets and triplets were acquired, as shown in Figure 8g–j. Because the majority of the

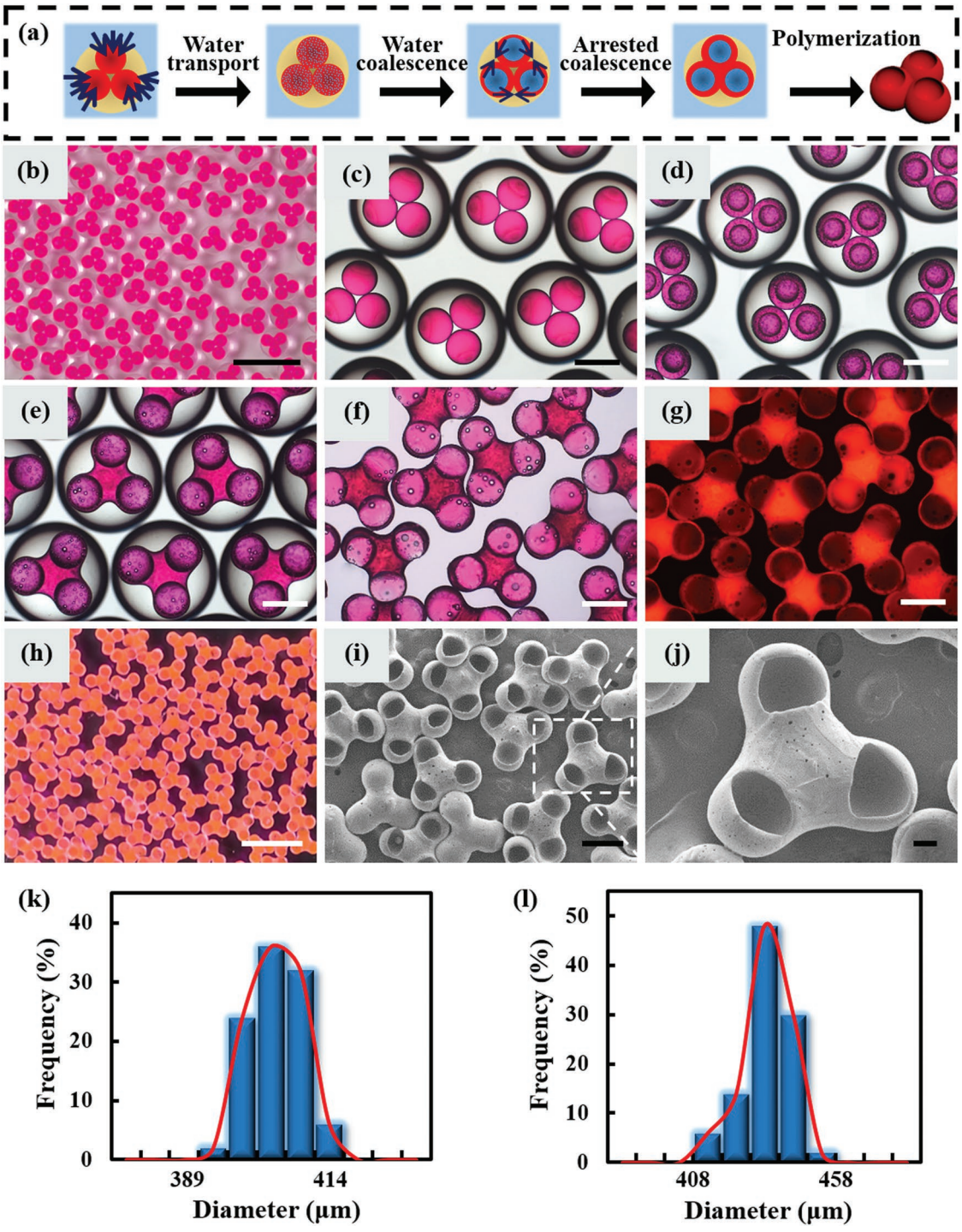

Figure 6. a) Schematic diagrams of arrested coalescence process of triple-core O/O/W double emulsions. b) Optical images of triple-core O/O/W double emulsions after collection, which can be produced on a large scale. c–e) Optical microscope images of triple-core O/O/W double emulsions after collection for c) 0 h, d) 1 h, and e) 10 h. f) Optical microscope images of PIL triplets after polymerization. g) Fluorescence microscope images of PIL triplets. h) Optical images of large amounts of PIL triplets. i,j) SEM images of the fabricated PIL triplets. k,l) Size distribution of inner cores in triple-core O/O/W double emulsions after k) collection and l) polymerization. Scale bars are 2 mm in (b), 500 μm in (c)–(g), 2 mm in (h), 500 μm in (i), and 100 μm in (j).

inner oil phase was unpolymerizable C_4mim[Tf_2N] and was removed by washing with ethanol, PETPTA doublets and triplets shrank after drying (see SEM images in Figure 8h,j). The ILs/salts system here just works as a template to create PETPTA nonspherical microparticles. All these results indicate that our ILs/salts system can serve as a versatile platform and that our strategy can be greatly extended to create various functional nonspherical materials, presenting tremendous application scope.

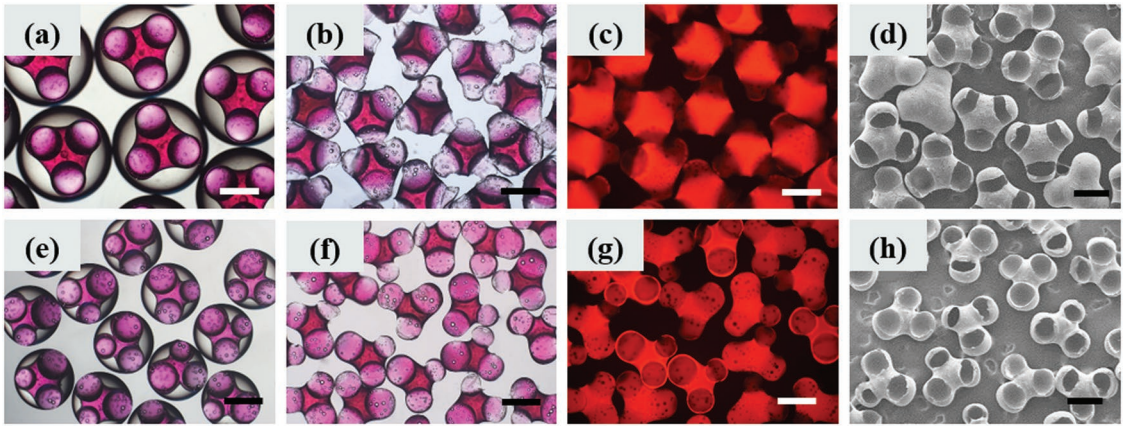

Figure 7. a) Optical microscope images of triple-core O/O/W double emulsions after collection for 22 h. b–d) Optical, fluorescence, and SEM images of PIL triplets of 22 h still standing. e) Optical microscope images of triple-core O/O/W double emulsions with cores of different sizes after collection for 10 h. f–h) Optical, fluorescence, and SEM images of scalene triangle PIL triplets. All scale bars are 500 µm.

2.5. Sequential Coalescence in Triple-Core O/O/W Double Emulsions Controlled by Osmotic Pressure Difference of Cores

To further exploit the value of osmosis-driven droplet coalescence, we used triple-core double emulsions to trigger sequential coalescence, which is of great importance for multistep microreactions in chemical and biological fields. **Figure 9** shows the time-lapse optical microscope images of a triple-core double emulsion with its cores experiencing sequential coalescence. The three cores were generated with almost the same volume but different salt concentrations and thus different osmotic pressures. In Figure 9a, the red-dyed (rhodamine B) core was of high salt concentration (IL:salt = 5:2), while the orange-dyed (methyl orange) core was of middle salt

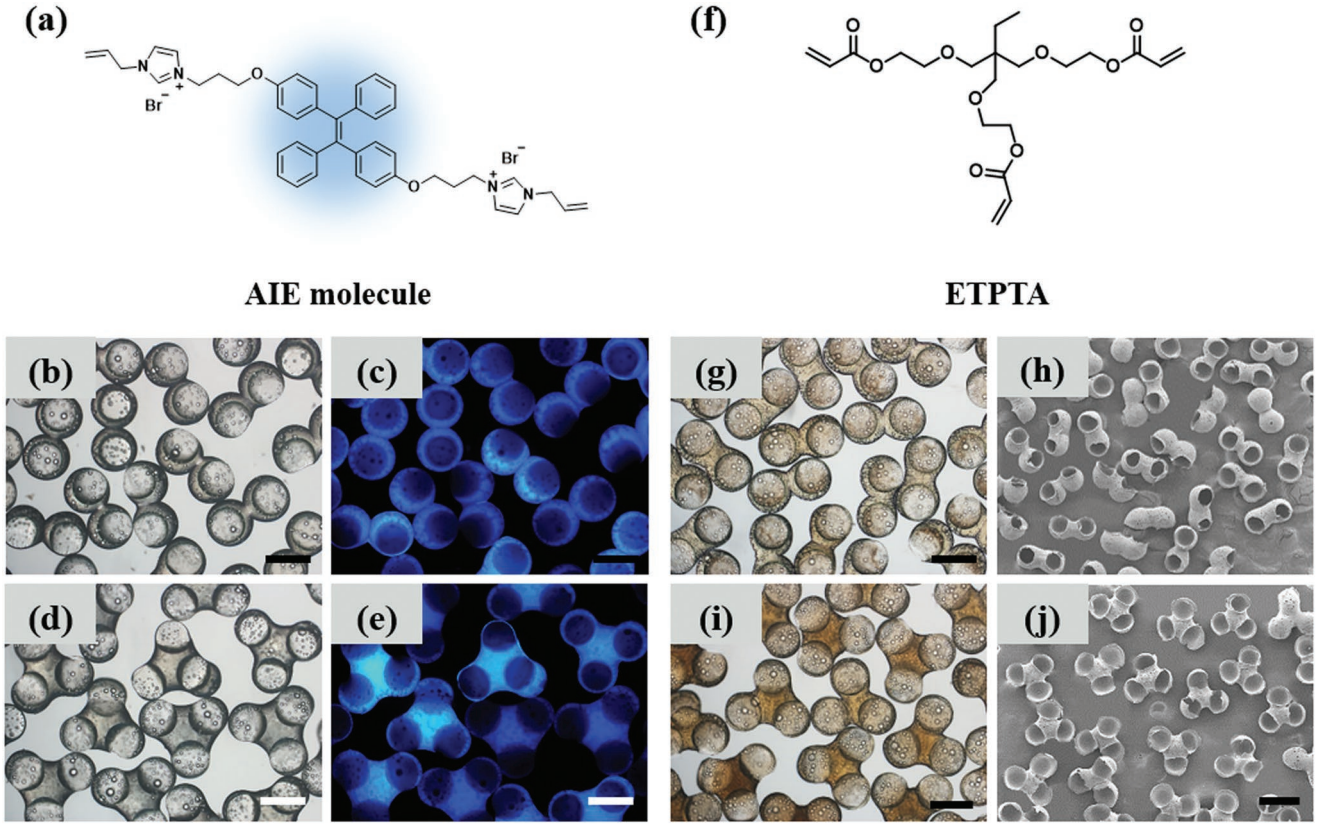

Figure 8. a) Chemical structure of the AIE molecule dissolved into the IL. b,c) Optical and fluorescence microscope images of PIL doublets doped with the AIE molecule. d,e) Optical and fluorescence microscope images of PIL triplets doped with the AIE molecule. f) Chemical structure of ETPTA. g,h) Optical and SEM images of PETPTA doublets. i,j) Optical and SEM images of PETPTA triplets. All scale bars are 500 µm.

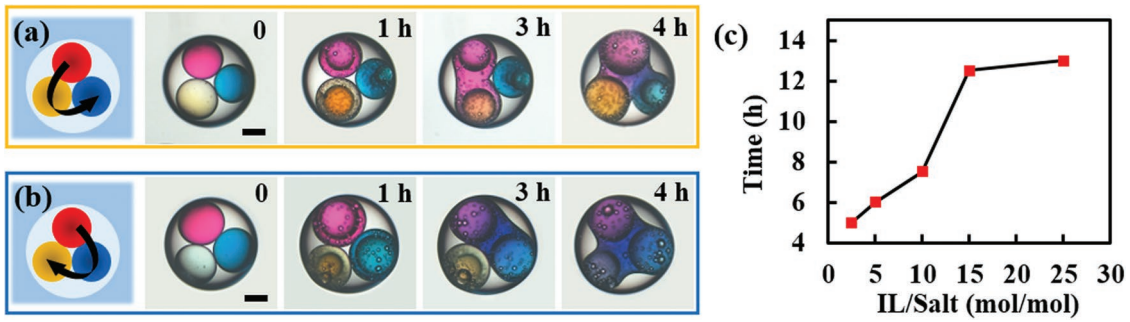

Figure 9. a,b) Time-lapse optical microscope images of a) counterclockwise and b) clockwise sequential coalescence in a triple-core double emulsion. The scale bar is 200 µm. c) Variation with IL/salt molecular ratio of coalescence time in dual-core O/O/W double emulsions.

concentration (IL:salt = 5:1) and the blue-dyed (methyl blue) core was of low salt concentration (IL:salt = 5:0.2). Consequently, the red core and the orange core coalesced first after 3 h. Then, the blue core merged together after another 1 h and dyes diffused into each other. Then the salt concentrations of the orange core and the blue core were interchanged, coalescence took place in the clockwise sequence (red–blue–orange) instead of counterclockwise sequence (red–orange–blue), as shown in Figure 9b. Therefore, coalescence sequence in triple-core double emulsions is programmed by controlling osmotic pressure difference of cores.

The sequential coalescence of the three cores in the triple-core double emulsion originates from the osmotic pressure difference caused by different concentrations of salts. The two cores containing more salts own high osmotic pressure and therefore absorb water more and in a faster speed. Therefore, the interface between two salt-rich cores is more unstable and coalescence prefers to take place between two salt-rich cores. To demonstrate this, we explored the effect of salt concentration on the coalescence time using dual-core double emulsions. As expected, with the increase of salt concentration, coalescence time between two inner cores decreased (Figure 9c). These results show the potential of the multi-core double emulsions as multistep microreactors regulated by osmotic pressure. Besides, as can be seen from Figure 9c, when the IL/salt molar ratio was more than 15:1, over 12 h were needed to start coalescence. To guarantee production efficiency, we presumed that the coalescence should take place within 12 h. Therefore, the maximum of IL/salt molar ratio was 15:1 and the corresponding minimum osmotic pressure of the ILs/salts (IL:salt = 15:1) was determined to be 1.1×10^4 kPa for efficient preparation of nonspherical microparticles.

3. Conclusion

In summary, a facile and high-throughput strategy to create nonspherical microparticles is developed through osmosis-driven arrested coalescence of emulsions. Based on microfluidic strategy, well-defined O/O/W double emulsions are first generated using C_4vim[Tf_2N]-LiTf_2N as the inner oil phase. In the ILs/salts system, osmosis-driven water transport and phase separation trigger spontaneous arrested coalescence of adjoining inner cores in O/O/W double emulsions, leading to nonspherical emulsions. The metastable state can last for several days because of high viscosity of the inner oil phase and new formed aqueous phase, which provides possibility to UV polymerize nonspherical emulsions to nonspherical microparticles. By adjusting the core number of O/O/W double emulsions, monodisperse dumbbell-like doublets and three-pointed star triplets are created. By tailoring coalescence time, more complex rod-like, spindle, and triangle microparticles are produced. Besides, anisotropic snowman-like doublets, tumbler-like doublets, and scalene triangle triplets are created by injecting multiple cores in O/O/W double emulsions. More importantly, benefitting from excellent solvency of ILs, our ILs/salts system could serve as a general platform to produce nonspherical microparticles made from different materials. What is more, sequential coalescence in triple-core double emulsions is programmed using the osmotic pressure difference, exhibiting the potential application in multistep chemical reactions. The strategy developed by us enables creation of a series of nonspherical microparticles through arrested coalescence of microfluidic emulsions with high productivity. And more interesting structures are supposed to be generated by extending our strategy to other microfluidic fabricated emulsions. To our knowledge, this is the first report of such fabrication strategy. The fabricated novel materials can be further used as new building blocks and microreactors for fundamental study and practical applications.

4. Experimental Section

Materials: All reagents and solvents were commercially available and used as received without further purification. 1-methylimidazole, 1-vinylimidazole, 1-bromobutane, PVA (M_w = 13 000–23 000 with 98% hydrolyzed), rhodamine B, methyl orange, and methyl blue were bought from Alfa Aesar. Bis(trifluoromethane)sulfonimide lithium, ETPTA, and photoinitiator HMPP were purchased from Sigma-Aldrich. Silicon oil (100 cSt) was bought from Yunuo Chemicals Ltd., China. PDMS (KF-96) was gained from ShinEtsu Chemical, Japan. Surfactant Dow Corning 749 was purchased from Dow Corning Company. Blue carbon dots were prepared according to reported procedures in literature.[64] AIE molecules were prepared according to reported procedures in literature.[65] All solvents were purchased from Beijing Chemical Company.

Synthesis of IL Monomers and Crosslinkers: C_4vim[Tf_2N] was synthesized according to reported procedures in literature with slight modification and used as the IL monomer.[66,67] Briefly, 1 molar equivalent 1-vinylimidazole was mixed with 1.1 molar equivalents

1-bromobutane and the mixture was vigorously stirred at 70 °C. After 12 h reaction, the mixture was washed with diethyl ether three times and dried to get 1-butyl-3-vinylimidazolium bromide (C_4vim[Br]). C_4vim[Br] was converted into C_4vim[Tf_2N] by adding LiTf_2N salt into aqueous solution of C_4vim[Br]. The formed C_4vim[Tf_2N] was washed with distilled water three times and dried to get the pure products. ^{1}H NMR (600 MHz, DMSO-d_6, δ): 9.46 (s, 1H), 8.18 (s, 1H), 7.91 (s, 1H), 7.26 (dd, J = 8.7 Hz, J = 15.6 Hz, 1H), 5.93 (dd, J = 2.4 Hz, J = 15.6 Hz, 1H), 5.41 (dd, J = 2.3 Hz, J = 8.7 Hz, 1H), 4.18 (t, J = 7.2 Hz, 2H), 1.84–1.75 (m, 2H), 1.34–1.23 (m, 2H), 0.90 (t, J = 7.4 Hz, 3H) (Figure S8, Supporting Information). The synthesis route of unpolymerizable 1-butyl-3-methylimidazolium bis(trifluoromethanesulfonyl)imide (C_4mim[Tf_2N]) was the same as C_4vim[Tf_2N], just replacing reactant 1-vinylimidazole with 1-methylimidazole. 1,6-di(*N*,*N*′-vinylimidazolium) hexane dibromide (D[vimC_6]Br) was prepared according to reported procedures in literature and used as the crosslinker.[68] Briefly, a mixture of 2 molar equivalents of 1-vinylimidazole and 1 molar equivalent of 1,6-dibromohexane was stirred at room temperature until the solution was solidified. Next, the solid was dissolved in methanol and washed with ethyl acetate three times to remove impurities. After that, the solid was dried under vacuum to get pure products. ^{1}H NMR (600 MHz, DMSO-d_6, δ): 9.67 (s, 2H), 8.24 (s, 2H), 7.98 (s, 2H), 7.32 (dd, J = 8.7 Hz, J = 15.6 Hz, 2H), 5.98 (dd, J = 2.4 Hz, J = 15.7 Hz, 2H), 5.42 (dd, J = 2.4 Hz, J = 8.7 Hz, 2H), 4.21 (t, J = 7.2 Hz, 4H), 1.97–1.71 (m, 4H), 1.30 (t, J = 7.0 Hz, 4H) (Figure S9, Supporting Information).

Fabrication of Microfluidic Devices and Droplet Formation: The capillary microfluidic devices were constructed from assembling of round and square glass capillaries on glass slides. The round glass capillary tubes (World Precision Instruments) with inner and outer diameters of 1.12 and 1.5 mm, respectively, were tapered using a flaming/brown micropipette puller (Sutter Instrument, P-97) and then grinded to around 600 µm to act as the injection channels for double emulsions' middle oil phase. The same round glass capillary tubes without tapering and grinding were used as the collection channels. The tapered and collection capillary were then coaxially inserted into a square capillary with inner diameter 1.75 mm (AIT Glass). Another small stretched capillary with diameter of about 100 µm was coaxially inserted into the tapered capillary to act as the injection channel of double emulsions' inner oil phase. When different inner oil phases were needed to inject, several small stretched capillaries were inserted into the tapered capillary accordingly. A transparent epoxy resin was used to seal the tubes where necessary (Figure S10, Supporting Information). C_4vim[Tf_2N]-LiTf_2N mixture, silicone oil phase, and PVA aqueous phase were injected into the small stretched capillaries, tapered round capillaries, and square capillaries as the inner oil phase, middle oil phase, and the outer phase, respectively. The flow rate of the inner oil phase, middle oil phase, and the outer phase were typically set at 0.05, 0.30, and 6.00 mL h^{-1}, respectively, for generation of single-core double emulsions. The flow rate of the outer phase was decreased to 3.50 and 1.40 mL h^{-1} for generation of dual-core and triple-core doubles emulsions, respectively. All fluids were pumped into the microfluidic device using syringe pumps (Harvard Apparatus).

Characterization: Optical microscope images of emulsions and microparticles were taken by an inverted microscope (Olympus, IX71) equipped with a CCD camera (OLYMPUS, DP73). The fluorescence microscope images were taken by the same inverted microscope using a mercury lamp (Olympus, U-RFL-T). Optical images of large amounts of samples were captured by Nikon digital camera. Interfacial tension was measured by DataPhysics OCA 15Pro. Viscosity was measured by Anton Paar Physica MCR301 at 25 °C. Images were analyzed and processed appropriately using ImageJ. The structure of microparticles was characterized using SEM (Hitachi, SU8010). ^{1}H NMR spectra were recorded on a 600 MHz NMR spectrometer (JNM-ECA600).

Determination of Osmotic Pressure of ILs/Salts: To determine the osmotic pressure of ILs/salts, the isotonic solution method was used. In detail, a series of ILs/salts droplets were immersed into respective aqueous solutions which contained gradient concentrations of NaCl by DataPhysics OCA 15Pro. If there existed osmotic difference between the ILs/salts drop and the NaCl aqueous solution, water transport and phase separation would take place and be observed by the microscope. If there exactly existed no osmotic difference, no water transport and phase separation would be observed. Therefore, the osmotic pressure of ILs/salts could be determined by calculating the osmotic pressure of the isotonic NaCl solution. In this work, the ILs/salts (IL:salt = 5:1, mol/mol) was isotonic with 2.875 mol L^{-1} NaCl aqueous solution. The corresponding osmotic pressure $P = 2cRT$ was calculated, where c is the concentration of the monovalent salt in the ideal solution, R is the gas constant, and T is the Kelvin temperature. As a result, the osmotic pressure of the ILs/salts (IL:salt = 5:1) was estimated to be 1.4×10^4 kPa.

Supporting Information

Supporting Information is available from the Wiley Online Library or from the author.

Acknowledgements

K.F. and N.G. contributed equally to this work. The authors gratefully acknowledge the financial support from the NSF China (nos. 21773135, 21473098, 21121004, and 21421064), MOST (2017YFA0204501, 2013CB834502), and the Deutsche Forschungsgemeinschaft DFG (TRR61).

Conflict of Interest

The authors declare no conflict of interest.

Keywords

arrested coalescence, ionic liquids, microfluidic emulsions, nonspherical microparticles, osmotic pressure

Received: July 19, 2019
Revised: August 23, 2019
Published online:

[1] Y. Qiu, K. Park, *Adv. Drug Delivery Rev.* **2001**, *53*, 321.
[2] S. C. Glotzer, M. J. Solomon, *Nat. Mater.* **2007**, *6*, 557.
[3] B. G. Chung, K. H. Lee, A. Khademhosseini, S. H. Lee, *Lab Chip* **2012**, *12*, 45.
[4] P. J. Yunker, T. Still, M. A. Lohr, A. G. Yodh, *Nature* **2011**, *476*, 308.
[5] L. Chen, H. Z. An, R. Haghgooie, A. T. Shank, J. M. Martel, M. Toner, P. S. Doyle, *Small* **2016**, *12*, 2001.
[6] J. Fan, S. H. Kim, Z. Chen, S. Zhou, E. Amstad, T. Lin, D. A. Weitz, *Small* **2017**, *13*, 1701256.
[7] A. S. Utada, E. l. Lorenceau, D. R. Link, P. D. Kaplan, H. A. Stone, D. A. Weitz, *Science* **2005**, *308*, 537.
[8] G. M. Whitesides, *Nature* **2006**, *442*, 368.
[9] P. N. Nge, C. I. Rogers, A. T. Woolley, *Chem. Rev.* **2013**, *113*, 2550.
[10] L. Shang, Y. Cheng, Y. Zhao, *Chem. Rev.* **2017**, *117*, 7964.
[11] M. J. Murray, M. J. Snowden, *Adv. Colloid Interface Sci.* **1995**, *54*, 73.
[12] M. Yoshida, K.-H. Roh, J. Lahann, *Biomaterials* **2007**, *28*, 2446.
[13] L. J. Bonderer, A. R. Studart, L. J. Gauckler, *Science* **2008**, *319*, 1069.
[14] B. Y. Shekunov, P. Chattopadhyay, H. H. Y. Tong, A. H. L. Chow, *Pharm. Res.* **2007**, *24*, 203.
[15] K. Jiang, C. Xue, C. Arya, C. Shao, E. O. George, D. L. DeVoe, S. R. Raghavan, *Small* **2011**, *7*, 2470.

[16] S. S. Lee, A. Abbaspourrad, S. H. Kim, *ACS Appl. Mater. Interfaces* **2014**, *6*, 1294.
[17] A. B. Subramaniam, M. Abkarian, L. Mahadevan, H. A. Stone, *Nature* **2005**, *438*, 930.
[18] M. Cui, T. Emrick, T. P. Russell, *Science* **2013**, *342*, 460.
[19] J. Forth, X. Liu, J. Hasnain, A. Toor, K. Miszta, S. Shi, P. L. Geissler, T. Emrick, B. A. Helms, T. P. Russell, *Adv. Mater.* **2018**, *30*, 1707603.
[20] M. F. Haase, K. J. Stebe, D. Lee, *Adv. Mater.* **2015**, *27*, 7065.
[21] D. Dendukuri, D. C. Pregibon, J. Collins, T. A. Hatton, P. S. Doyle, *Nat. Mater.* **2006**, *5*, 365.
[22] D. Dendukuri, S. S. Gu, D. C. Pregibon, T. A. Hatton, P. S. Doyle, *Lab Chip* **2007**, *7*, 818.
[23] J. H. Jang, D. Dendukuri, T. A. Hatton, E. L. Thomas, P. S. Doyle, *Angew. Chem., Int. Ed.* **2007**, *46*, 9027.
[24] S. Guo, T. Yao, X. Ji, C. Zeng, C. Wang, L. Zhang, *Angew. Chem., Int. Ed.* **2014**, *53*, 7504.
[25] J. Wang, L. Shang, Y. Cheng, H. Ding, Y. Zhao, Z. Gu, *Small* **2015**, *11*, 3890.
[26] M. J. Zhang, W. Wang, X. L. Yang, B. Ma, Y. M. Liu, R. Xie, X. J. Ju, Z. Liu, L. Y. Chu, *ACS Appl. Mater. Interfaces* **2015**, *7*, 13758.
[27] S. N. Yin, S. Yang, C. F. Wang, S. Chen, *J. Am. Chem. Soc.* **2016**, *138*, 566.
[28] L. Wang, M. Qiu, Q. Yang, Y. Li, G. Huang, M. Lin, T. J. Lu, F. Xu, *ACS Appl. Mater. Interfaces* **2015**, *7*, 11134.
[29] M. Li, Q. Yang, H. Liu, M. Qiu, T. J. Lu, F. Xu, *Small* **2016**, *12*, 4492.
[30] C. Ohm, N. Kapernaum, D. Nonnenmacher, F. Giesselmann, C. Serra, R. Zentel, *J. Am. Chem. Soc.* **2011**, *133*, 5305.
[31] A. R. Studart, H. C. Shum, D. A. Weitz, *J. Phys. Chem. B* **2009**, *113*, 3914.
[32] A. B. Pawar, M. Caggioni, R. Ergun, R. W. Hartel, P. T. Spicer, *Soft Matter* **2011**, *7*, 7710.
[33] P. Dahiya, A. DeBenedictis, T. J. Atherton, M. Caggioni, S. W. Prescott, R. W. Hartel, P. T. Spicer, *Soft Matter* **2017**, *13*, 2686.
[34] H. C. Shum, A. R. Abate, D. Lee, A. R. Studart, B. Wang, C. H. Chen, J. Thiele, R. K. Shah, A. Krummel, D. A. Weitz, *Macromol. Rapid Commun.* **2010**, *31*, 108.
[35] P. Atkins, J. de Paula, *Atkins' Physical Chemistry*, Oxford University Press, Oxford **2014**.
[36] V. W. Sidel, A. K. Solomon, *J. Gen. Physiol.* **1957**, *41*, 243.
[37] E. L. Fiscus, *Plant Physiol.* **1975**, *55*, 917.
[38] Y. C. Kim, M. Elimelech, *J. Membr. Sci.* **2013**, *429*, 330.
[39] C. X. Guo, D. Zhao, Q. Zhao, P. Wang, X. Lu, *Chem. Commun.* **2014**, *50*, 7318.
[40] S. H. Kim, J. G. Park, T. M. Choi, V. N. Manoharan, D. A. Weitz, *Nat. Commun.* **2014**, *5*, 3068.
[41] S. J. Yeo, F. Tu, S. H. Kim, G. R. Yi, P. J. Yoo, D. Lee, *Soft Matter* **2015**, *11*, 1582.
[42] Y. Chao, S. Y. Mak, S. Rahman, S. Zhu, H. C. Shum, *Small* **2018**, *14*, 1802107.
[43] X. Guan, L. Hou, Y. Ren, X. Deng, Q. Lang, Y. Jia, Q. Hu, Y. Tao, J. Liu, H. Jiang, *Biomicrofluidics* **2016**, *10*, 034111.
[44] L. Hou, Y. Ren, Y. Jia, X. Chen, X. Deng, Z. Tang, Q. Hu, Y. Tao, H. Jiang, *Microfluid. Nanofluid.* **2017**, *21*, 60.
[45] N. Jager-Lezer, I. Terrisse, F. Bruneau, S. Tokgoz, L. Ferreira, D. Clausse, M. Seiller, J. L. Grossiord, *J. Controlled Release* **1997**, *45*, 1.
[46] S. Geiger, S. Tokgoz, A. Fructus, N. Jager-Lezer, M. Seiller, C. Lacombe, J. L. Grossiord, *J. Controlled Release* **1998**, *52*, 99.
[47] N. Gao, J. Cui, W. Zhang, K. Feng, Y. Liang, S. Wang, P. Wang, K. Zhou, G. Li, *Chem. Sci.* **2019**, *10*, 7887.
[48] T. H. Niepa, L. Hou, H. Jiang, M. Goulian, H. Koo, K. J. Stebe, D. Lee, *Sci. Rep.* **2016**, *6*, 30578.
[49] M. J. Monteiro, F. F. Bazito, L. J. Siqueira, M. C. Ribeiro, R. M. Torresi, *J. Phys. Chem. B* **2008**, *112*, 2102.
[50] M. Y. Lui, L. Crowhurst, J. P. Hallett, P. A. Hunt, H. Niedermeyer, T. Welton, *Chem. Sci.* **2011**, *2*, 1491.
[51] A. B. Pereiro, J. M. M. Araújo, F. S. Oliveira, J. M. S. S. Esperança, J. N. Canongia Lopes, I. M. Marrucho, L. P. N. Rebelo, *J. Chem. Thermodyn.* **2012**, *55*, 29.
[52] V. L. Martins, B. G. Nicolau, S. M. Urahata, M. C. Ribeiro, R. M. Torresi, *J. Phys. Chem. B* **2013**, *117*, 8782.
[53] T. Welton, *Chem. Rev.* **1999**, *99*, 2071.
[54] R. D. Rogers, K. Seddon, *Science* **2003**, *302*, 792.
[55] R. Shi, Y. Wang, *Sci. Rep.* **2016**, *6*, 19644.
[56] J. Wang, Y. Hu, R. Deng, W. Xu, S. Liu, R. Liang, Z. Nie, J. Zhu, *Lab Chip* **2012**, *12*, 2795.
[57] V. Chokkalingam, Y. Ma, J. Thiele, W. Schalk, J. Tel, W. T. Huck, *Lab Chip* **2014**, *14*, 2398.
[58] M. Y. Koroleva, E. V. Yurtov, *J. Colloid Interface Sci.* **2006**, *297*, 778.
[59] S. Torza, T. G. Mason, *Science* **1969**, *163*, 813.
[60] A. Loxley, B. Vincent, *J. Colloid Interface Sci.* **1998**, *208*, 49.
[61] S.-H. Kim, H. Hwang, C. H. Lim, J. W. Shim, S.-M. Yang, *Adv. Funct. Mater.* **2011**, *21*, 1608.
[62] J. T. Wang, J. Wang, J. J. Han, *Small* **2011**, *7*, 1728.
[63] C. H. Choi, J. Kim, J. O. Nam, S. M. Kang, S. G. Jeong, C. S. Lee, *ChemPhysChem* **2014**, *15*, 21.
[64] X. Miao, D. Qu, D. Yang, B. Nie, Y. Zhao, H. Fan, Z. Sun, *Adv. Mater.* **2018**, *30*, 1704740.
[65] W. Zhang, N. Gao, J. Cui, C. Wang, S. Wang, G. Zhang, X. Dong, D. Zhang, G. Li, *Chem. Sci.* **2017**, *8*, 6281.
[66] T. Kakibe, H. Ohno, *J. Mater. Chem.* **2009**, *19*, 4960.
[67] M. A. Ab Rani, A. Brant, L. Crowhurst, A. Dolan, M. Lui, N. H. Hassan, J. P. Hallett, P. A. Hunt, H. Niedermeyer, J. M. Perez-Arlandis, M. Schrems, T. Welton, R. Wilding, *Phys. Chem. Chem. Phys.* **2011**, *13*, 16831.
[68] J. Cui, N. Gao, J. Li, C. Wang, H. Wang, M. Zhou, M. Zhang, G. Li, *J. Mater. Chem. C* **2015**, *3*, 623.